This article has been accepted for publication in a future issue of this journal, but has not been fully edited. Content may change prior to final publication. Citation information: DOI 10.1109/TNS.2019.2943597, IEEE Transactions on Nuclear Science

A solid-state microdosimeter for dose and radiation quality monitoring for astronauts in space

S. Peracchi, L. T. Tran, B. James, D. Bolst, D. A. Prokopovich, J. A. Davis, S. Guatelli, M. Petasecca, M. L. F. Lerch, N. Matsufuji, A. Kok, M. Povoli, M. Jackson and A. B. Rosenfeld

***Abstract* – This paper presents a study of the response of the silicon on insulator (SOI) microdosimeter with 3-dimensional (3D) sensitive volumes (SV) to 400 MeV/u ^{16}O and 500 MeV/u ^{56}Fe ions mimicking Galactic Cosmic Rays outside and inside the International Space Station (ISS). An average quality factor ($\bar{Q}$) and the dose equivalent (*H*) of the radiation field were obtained experimentally and the results were compared with GEANT4 simulations.**

Keywords – SOI microdosimeter, ISS, GCR, heavy ions.

I. Introduction

Space exploration is currently aiming to reach further destinations, increasing astronauts' exposure to hazardous radiation. The dose equivalent, H, is a quantity which expresses the probability that exposure to ionizing radiation will cause biological effects. It is obtained by multiplying the dose by the quality factor, Q, of the radiation.

At the altitude of the International Space Station (ISS), the main radiation sources are Galactic Cosmic Rays (GCR), made up of approximately 87% protons, 12% alpha particles and 1% heavy ions (e.g. C, O, Si, Fe) with a wide energy range, up to hundreds of GeV/n; [1, 2]. Although the heavier ions' abundance is much lower than protons and alpha particles, their high LET makes them strong contributors for radiobiological effects on humans. Moreover, while high energy ions traversing the spacecraft materials and tissue, the secondary particles are produced significantly.

Microdosimetry is a useful approach for evaluating the Q of a mixed radiation field typical of space radiation, without knowing the energy or type of particles. Such measurements are currently available on the ISS using the conventional Tissue Equivalent Proportional Counter (TEPC), which is bulky, requires a high voltage supply and cannot be used as a personal dosimeter for astronauts [3]. Portable and low power devices are preferable since an astronaut's location inside the ISS changes and the composition and dose rate of the radiation field is not predictable. The Medipix track detector is a portable device currently used on the ISS [4]. However, it requires software for individual track analysis which is complex to convert the measured response to dose equivalent.

SOI microdosimeters provide many advantages over both TEPCs and track-type detectors in terms of both portability and simple a readout and data processing system.

In this work, an SOI microdosimeter with 3D sensitive volumes (SVs) is used to study the effect of the ISS wall on the Q and dose equivalent when irradiated with ^{16}O and ^{56}Fe ions. These measurements are presented in terms of dose at 0.07 mm (Hp(0.07)) and 10 mm (Hp(10)) [5] below a specified point in an astronaut, represented in this study by a water phantom. Measurements at different depths in water, mimicking different positions in the astronaut's body, were also performed. A Monte Carlo simulation using Geant4 was done to compare to the experimental measurements. The SOI microdosimeter used in this study was developed by the Centre for Medical Radiation Physics (CMRP), University of Wollongong in collaboration with the nanofabrication foundry SINTEF, Norway.

II. Materials and Methods

A. The 3D "mushroom" SOI microdosimeter

Since the 90s, the CMRP has been active in the development of SOI microdosimeters, as an alternative to TEPCs, for radiation protection purposes [6]. The SOI microdosimeter used in this experiment consists of a matrix of silicon SVs with dimensions of a biological cell. In this study, an SOI "mushroom" design microdosimeter was used, which has an array of 400 cylindrical SVs consisting of n^+ planar electrodes surrounded by p^+ trench electrodes [7, 8]. The SV has dimensions of 18 µm in diameter and 10 µm in height and the distance between two adjacent SVs is 50 µm (pitch) (Figure 1).

S. Peracchi, B. James, L. T. Tran, D. Bolst, J. Davis, S. Guatelli, M. Petasecca, M. Lerch, and A. B. Rosenfeld are with the Centre for Medical Radiation Physics, University of Wollongong, Wollongong, NSW 2087, Australia (e-mail: sp009@uowmail.edu.au; bj197@uowmail.edu.au; tltran@uow.edu.au; db001@uowmail.edu.au; jeremyd@uow.edu.au; susanna@uow.edu.au; marcop@uow.edu.au; mlerch@uow.edu.au; anatoly@uow.edu.au). D. Prokopovich is with Australia's Nuclear Science and Technology Organisation, Lucas Heights, NSW 2234, Australia (e-mail: dale.prokopovich@ansto.gov.au). N. Matsufuji is with National Institutes for Quantum and Radiological Science and Technology, Chiba, Japan (e-mail: matsufuji.naruhiro@qst.go.jp). A. Kok and M. Povoli are with SINTEF MiNaLab, Gaustadalleen 23C, Oslo 0314, Norway (e-mail: Angela.Kok@sintef.no; Marco.Povoli@sintef.no). Michael Jackson is with the University of New South Wales, Sydney, NSW 2052, Australia (e-mail: michael.jackson@sydney.edu.au).

This article has been accepted for publication in a future issue of this journal, but has not been fully edited. Content may change prior to final publication. Citation information: DOI 10.1109/TNS.2019.2943597, IEEE Transactions on Nuclear Science

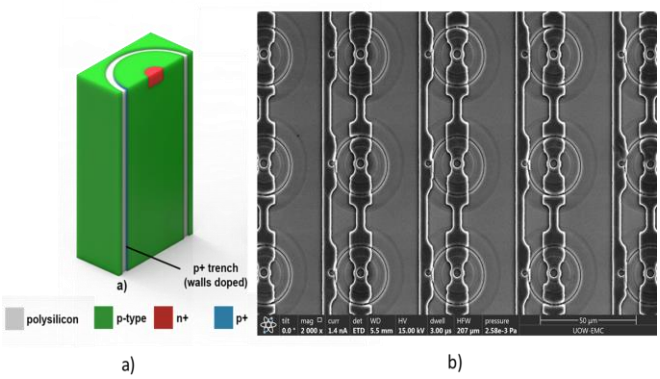

Figure 1. a) Simplified schematics illustrating sensitive volume geometry of a trenched planar structure and b) scanning electron microscope (SEM) image of the "mushroom" microdosimeter.

B. Q and H derivation from microdosimetric measurements

Microdosimetry involves measuring the stochastic energy deposition in SVs, on an event-by-event basis by primary and secondary particles. The microdosimetry quantity that can be experimentally measured is the lineal energy *y* given by:

$$y = \frac{E}{\langle l \rangle} \tag{1}$$

where *E* is the energy deposited in a SV with an average chord length <*l*>, which in our case was 10 µm, the thickness of the silicon SVs. The microdosimetric spectra *yd(y) vs y* in logarithmic scale can be derived from the measured frequency distribution *f(y)* and the dose lineal energy distribution *d(y)* as described elsewhere [9].

Through the analysis of the microdosimetric spectra, it is possible to calculate the quality factor Q of the radiation field of interest. Q is intended to relate the relative biological effectiveness (RBE) a specific radiation environment would cause to the human body. Q can be calculated with the formula provided by the ICRP Publication 60 [2]:

$$Q(LET) = \begin{Bmatrix} 1 & LET < 10 \\ 0.32LET - 2.2 & 10 \leq LET \leq 100 \\ 300\ LET^{-1/2} & LET > 100 \end{Bmatrix} \tag{2}$$

In equation (2), *LET* refers to the unrestricted linear energy transfer, in this work the lineal energy (Equation (1)) is used to calculate the quality factor instead of *LET*. *LET* and *y* will not differ significantly except for relatively low LET radiation such as protons with an energy of ~100 MeV or higher. At these energies of protons, the range of delta electrons in water is much larger than the size of the sensitive volume.

The value of *H* is obtained as follows:

$$H = D_{TE} * \bar{Q} \tag{3}$$

where D_{TE} is the absorbed dose in tissue, calculated by multiplying the absorbed dose in silicon D_{Si} by the tissue-equivalent factor 0.58 obtained from tissue equivalency studies in mixed fields of secondary charged particles [10-12] as follow:

$$D_{TE} = D_{Si} * 0.58. \tag{4}$$

We normalized the dose equivalent H per unit absorbed dose in water (per Gy) delivered at the Bragg Peak (BP). This normalization was applied to all dose calculations for the irradiations with iron and oxygen ions.

For astronauts' individual monitoring, we evaluate the personal dose equivalent Hp(d) defined as the dose equivalent in tissue at a depth "d" in a human body below the position where an individual dosimeter is worn. Consequently, Hp(0.07) and Hp(10) are the personal dose equivalents at a depth of 0.07 mm and 10 mm, respectively, below the skin, of a human body. To calculate these two quantities, we used two Poly(methyl methacrylate) (PMMA) converters 0.07 mm and 10 mm thick as an approximation of the ICRU human tissue [14] during the measurements in the free air geometry, which were placed on top of the SVs.

C. Experimental set-up

Irradiations were carried out at the Heavy Ions Medical Accelerator in Chiba (HIMAC) using a passive scattering beam of 400 MeV/u ^{16}O and 500 MeV/u ^{56}Fe. For the ^{16}O ion beam a 0.910 mm thick tantalum scatterer was used while for the ^{56}Fe ion beam a combination of a 0.215 mm thick tantalum scatter and a 1.60 mm thick lead scatterer were used. Detailed information of the beamline can be found elsewhere [13]. A field size of 5 × 5 cm^2 was produced using a 5 cm thick X-Y brass collimator placed at 140 mm upstream of the iso-center.

a. Free air geometry measurements

The SOI microdosimeter is connected to a low noise spectroscopy based readout electronics probe, named the MicroPlus (μ^+) probe (Figure 2b).

A free air geometry was implemented by placing the MicroPlus (μ^+) probe with the "mushroom" microdosimeter along the central axis of the beam, as shown in Figure 2 [14]. Two PMMA converters of 0.07 mm and 10 mm thick were put in front of the probe to reproduce the scenario for the personal dose equivalent Hp(0.07) and Hp(10) estimation, respectively.

Because the aim was to mimic the radiation environment outside and inside the ISS, the spacecraft's wall was modeled with two aluminum slabs corresponding to the ISS wall's specification [15, 16]: the first slab of 7.3 mm represents the real aluminum pressurized shell of the ISS. The thicker slab of 35.95 mm includes an additional layer corresponding to the so-called "Internal Out-fitting": it is considered as the equivalent areal mass of aluminum due to the presence of several devices and structures inside the habitable volume of the ISS. Although they are not homogeneously distributed inside the spacecraft, they provide a further barrier and source of additional secondaries to particle's radiation.

This article has been accepted for publication in a future issue of this journal, but has not been fully edited. Content may change prior to final publication. Citation information: DOI 10.1109/TNS.2019.2943597, IEEE Transactions on Nuclear Science

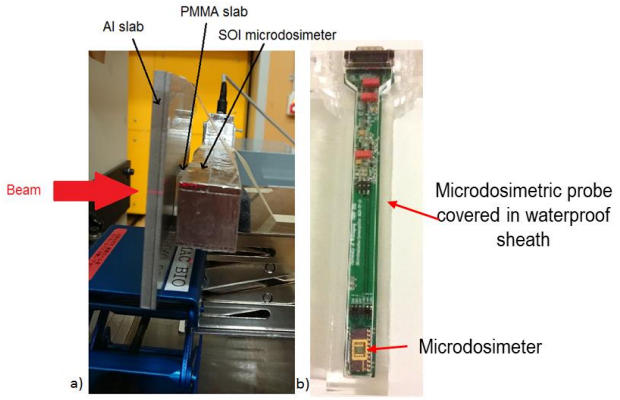

Figure 2. a) Free air geometry setup inside the irradiation room at HIMAC. b) SOI mushroom microdosimeter connected to the microdosimetric probe which is inserted into a waterproof sheath

b. *Measurements in a water phantom*

To mimic how $\bar{Q}$ and H change at different positions in an astronaut's body, we measured the microdosimetric response of the microdosimeter at different depths in a water phantom, representing the astronaut. The position of the MicroPlus (μ^+) probe's in a water phantom was controlled remotely using an X-Ymotion stage developed in house (Figure 3) [14]. The μ^+ probe was moved along the Y-axis in the beam's central axis with the beam incident on the top of the cylindrical SVs of the microdosimeter. The position of the μ^+ probe in the water phantom corresponds to "depth" in the astronaut's body. Thus, in our study we approximated the human body as made of water, with density 1 g/cm^3. If a heterogeneous composition is considered, then the depth should be corrected by the corresponding value of the density. Due to mechanical constraints, the minimum water equivalent depth achievable in the water phantom is 11.17 mm, referred to as the "entrance depth".

This study compares the microdosimetric spectra measured inside (with Al wall) and outside (no Al wall) of the spacecraft for an astronaut. Particularly, we used the 35.95 mm Al slab for oxygen ions measurements and only the thin 7.3 mm Al slab for iron ions because the thick 35.95 mm thick would have stopped the primary beam, before reaching the water phantom.

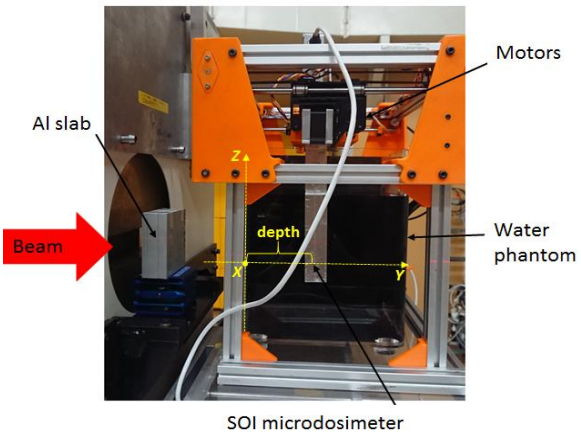

Figure 3. Water phantom geometry setup inside the irradiation room at HIMAC, with 35.95mm thick Al slab for the particular case of oxygen ions.

c. *GEANT4 validation*

A Geant4 simulation was developed based on the passive biological beamline model at HIMAC, validated through experimental measurements by (Bolst et al., 2019) [13]. The model reproduces the exact set up used during experiments, discussed in the previous paragraphs. Geant4 version 10.02p3 was adopted with the following physics list: *G4StandardOption3* to describe electromagnetic interactions, *Binary Intranuclear Cascade (BIC)* for hadronic interactions and *G4HadronElasticPhysicsHP* for elastic scattering of hadrons.

III. Results

A. *Free air geometry measurements*

Figure 4 shows tissue-equivalent microdosimetric spectra measured with the 3D "mushroom" SOI microdosimeter and their derived Q average value ($\bar{Q}$) for 500 MeV/u ^{56}Fe ions. The introduction of the 7.3 mm wall does not significantly change the microdosimetric spectra measured behind 0.07 mm and 10 mm of PMMA, which is dominated by primary ^{56}Fe ions. The corresponding $\bar{Q}$ values without/with 7.3 mm of Al wall were 23.38 and 22.69, respectively with the 0.07 mm PMMA converter and 22.97 and 22.10, respectively with the 10 mm PMMA converter. For an Al wall thickness of 35.95 mm, the primary ^{56}Fe ions are fully stopped, and the radiation field inside of the spacecraft is determined by secondary fragments and neutrons originated from the Al wall. As can be seen, the microdosimetric spectra obtained with the thick Al wall is broader in comparison with the lineal energy spectrum from the thin Al wall. This is due to the contribution of secondary particles generated inside the Al wall from the primary beam, producing lower $\bar{Q}$ values of 14.63 and 17.35 with two PMMA converters of 0.07 mm and 10 mm, respectively. The values of Hp(0.07) and Hp(10) were calculated based on the microdosimetric spectra and is shown in TABLE I. When the thick wall of Al was placed in front of the microdosimeter, ^{56}Fe ions are fully absorbed, the dose equivalent values dropped dramatically. The personal dose equivalent at the skin Hp(0.07) was calculated to be three times higher than the dose at 10 mm depth in tissue. It can be noted while personal dose equivalent at depth 10mm was reduced in comparison to the dose equivalent at depth 0.07mm, the $\bar{Q}$ is increased essentially owing to modification of secondary particles' spectrum propagated with depth. Microdosimetric spectra measured with the mushroom microdosimeter reveal to be themselves very sensitive to these changes with depth in water.

This article has been accepted for publication in a future issue of this journal, but has not been fully edited. Content may change prior to final publication. Citation information: DOI 10.1109/TNS.2019.2943597, IEEE Transactions on Nuclear Science

TABLE I

DOSE EQUIVALENT CALCULATED BASED ON THE MICRODOSIMETRIC SPECTRA FOR MEASUREMENTS IN FREE AIR.

500 MeV/u ^{56}Fe		
	Hp(0.07) (Sv/Gy)	Hp(10) (Sv/Gy)
No Al	1.99	1.93
7.3mm Al	1.97	1.92
35.95mm Al	0.43	0.13
400 MeV/u ^{16}O		
	Hp(0.07) (Sv/Gy)	Hp(10) (Sv/Gy)
No Al	0.47	0.45
35.95mm Al	0.54	0.56

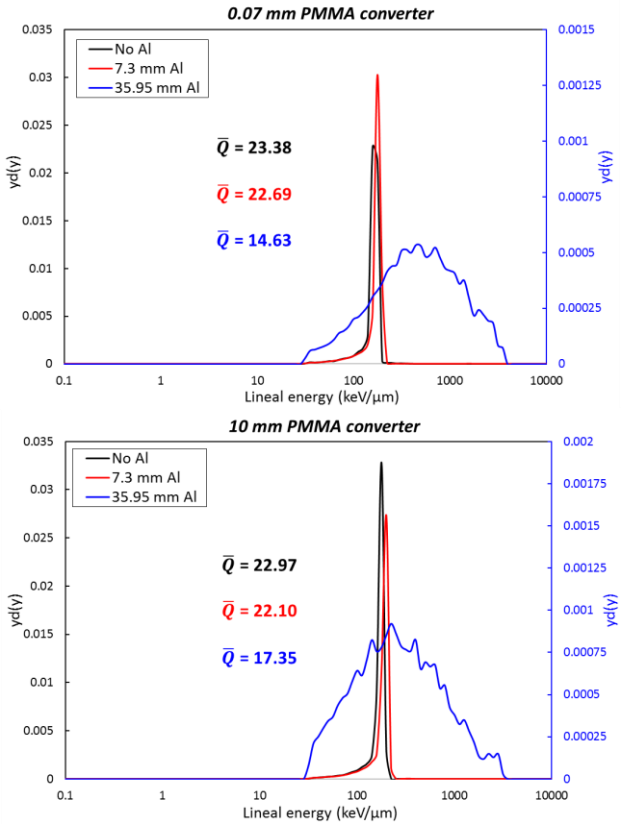

Figure 4. Microdosimetric spectra obtained during 500MeV/u ^{56}Fe irradiations in free air with two PMMA converters of 0.07mm thickness (top) and 10mm thickness (bottom).

Similarly, Figure 5 shows tissue-equivalent microdosimetric spectra measured with the 3D mushroom SOI microdosimeter for 400 MeV/u ^{16}O ions. In this case, the oxygen ions can penetrate the thick wall of 35.95 mm without being fully stopped, due to the higher range in water of 400 MeV/u ^{16}O ions compared to 500 MeV/u ^{56}Fe ions (Figure 4). When considering the 35.95 mm thick aluminum wall, the $\bar{Q}$ increases from 3.82 to 4.66, with 0.07 mm thick PMMA and from 3.84 to 4.83 with 10 mm thick PMMA converter. Derived Hp(0.07) and Hp(10) are also increased and show how harmful the field of ^{16}O ions is, particularly it is worse inside the spacecraft for this particular energy of ion which is not stopped in the wall, reducing the energy of the O ions and increasing higher LET after passing through the Al wall and converter.

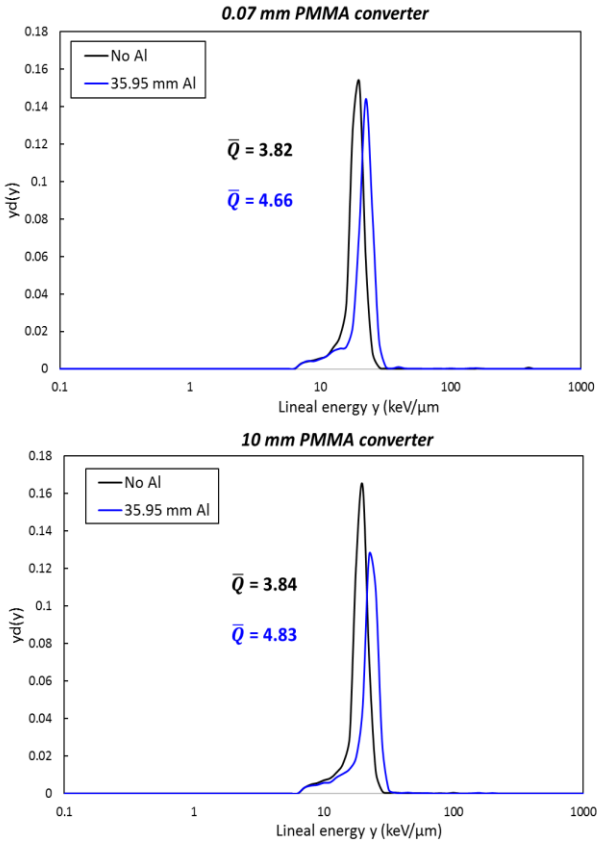

Figure 5. Microdosimetric spectra obtained during 400MeV/u ^{16}O irradiations in free air with two PMMA converters of 0.07mm thickness (top) and 10mm thickness (bottom).

GEANT4 simulations in free air geometry provide a good agreement with the experimental results in terms of $\bar{Q}$ (TABLE II). However, slight differences in values are due to statistics confirmed by the high error attributed to simulation. Therefore, for all simulations results we adopted the error obtained for measurements with the thick aluminum wall (35.95 mm), as the worst statistical case. In addition, an example of comparison of the experiment and simulation microdosimetric spectra is shown in Figure 6, where the matching between experimental and simulated peaks can be observed.

TABLE II

$\bar{Q}$ VALUES OBTAINED FROM EXPERIMENT AND SIMULATION IN FREE AIR GEOMETRY WITH 10mm PMMA CONVERTER.

500 MeV/u ^{56}Fe		
	$\bar{Q}$ Experiments	$\bar{Q}$ Simulation
No Al	22.97 ± 0.14	21.08 ± 1.28
7.3mm Al	22.10 ± 0.14	20.51 ± 1.28
35.95 Al	17.35 ± 0.18	16.32 ± 1.28
400 MeV/u ^{16}O		
	$\bar{Q}$ Experiments	$\bar{Q}$ Simulation
No Al	3.84 ± 0.04	3.78 ± 0.23
35.95 Al	4.83 ± 0.05	4.48 ± 0.23

This article has been accepted for publication in a future issue of this journal, but has not been fully edited. Content may change prior to final publication. Citation information: DOI 10.1109/TNS.2019.2943597, IEEE Transactions on Nuclear Science

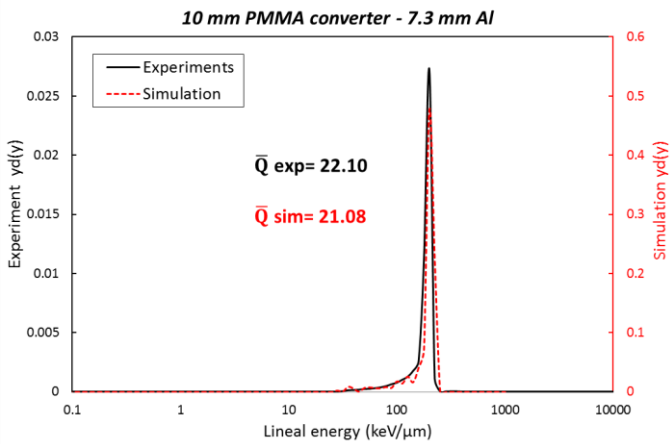

Figure 6. Example of microdosimetric spectra comparison from experiments and GEANT4 simulation: 500MeV/u ^{56}Fe irradiations in free air with 10 mm thick PMMA converter and Al wall of 7.3 mm thickness.

TABLE III

DOSE EQUIVALENT CALCULATED BASED ON THE MICRODOSIMETRIC SPECTRA FOR MEASUREMENTS IN WATER WITH AND WITHOUT THE AL WALL.

400 MeV/u ^{16}O		
Depth (mm)	H – No Al (Sv/Gy)	H – 35.95mm Al (Sv/Gy)
20	0.07	0.16
50	0.12	1.21
90	0.12	11.00
110	0.13	1.05
120	0.16	0.03

500 MeV/u ^{56}Fe			
Depth (mm)	H – No Al (Sv/Gy)	Depth (mm)	H – 7.3 mm Al (Sv/Gy)
20	3.88	11.17	6.42
		44.46	7.37
50	4.06	55.58	5.01
		57.33	11.44
62	4.47	62.6	1.63

B. *Water phantom measurements*

Figure 7 shows the trend of $\bar{Q}$ at different depths in water obtained during irradiation with 400 MeV/u ^{16}O. When no Al wall is considered (outside of the spacecraft scenario), the *LET* of oxygen ions entering the water phantom is 19.38 keV/µm, according to Equation (2) the $\bar{Q}$ value increases along depths in the body until 184 mm, corresponding to the BP position. The astronaut's body will be exposed mostly to primary oxygen ions until they stop at the BP and consequently, the dose will be due to fragments and other secondary particles produced downstream of the BP. Nevertheless, with the presence of the aluminum wall 35.95 mm thick, the O ions have a range of 110 mm in water. For the depths before 110 mm the $\bar{Q}$ values are higher if the astronaut is inside the spacecraft, representing a more harmful situation for the space crew.

When comparing the two scenarios, we can observe that oxygen ions are more harmful at deeper depths in the body if the astronaut was outside the spacecraft because of the increasing trend of $\bar{Q}$. If the astronaut was inside the spacecraft, the shielding of the wall would cause a shift of the Bragg Peak to a more superficial depth, causing a higher $\bar{Q}$ at the entrance of the body. The same ascendant trend was observed for the dose equivalent *H* (TABLE III): at 90mm depth in the body, the dose behind the spacecraft's wall is almost 100 higher per Gy delivered at the BP in water than considering an astronaut outside the spacecraft.

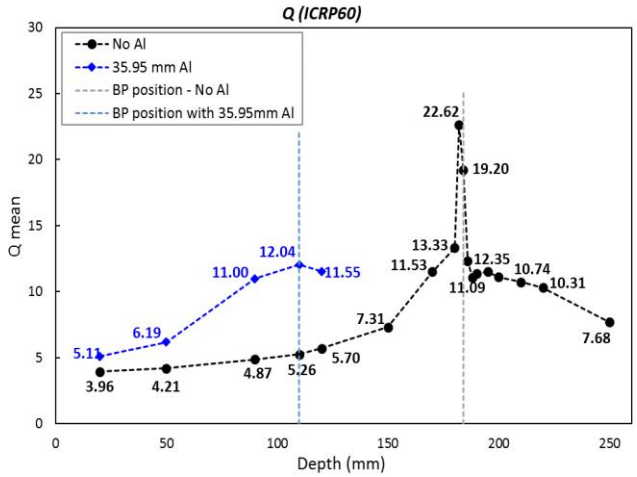

Figure 7. Quality factor $\bar{Q}$ at same depths in water with and without Al wall, obtained with SOI microdosimeter in response to 400 MeV/u ^{16}O ions. Vertical dashed lines show the Brag Peak position at 110 mm depth in water and 184 mm depth in water, respectively with 35.95 mm Al wall and without.

The same measurement was carried out with 500 MeV/u ^{56}Fe ions for an Al wall thickness of 7.3 mm and the corresponding $\bar{Q}$ trend is shown in Figure 8. In contrast to the oxygen ions, when no Al wall is considered (outside of the spacecraft scenario), $\bar{Q}$ decreases with depths until 75 mm, corresponding to the BP position. According to Equation (2), this behavior can be explained by the high *LET* of primary iron ions entering the water phantom being 167.98 keV/µm and further increasing with depth, which is much higher than the *LET* of 19.38 keV/µm at the entrance depth observed for oxygen ions. Therefore, $\bar{Q}$ is decreasing with depth upstream of the BP according to Q behaviour for *LET*>100keV/ µm as in Equation (2). Downstream of the BP, where the radiation field is due to fragmented primary iron ions and neutrons with lower *LET*, $\bar{Q}$ increases according to Equation (2) for *LET* <100keV/µm.

Nevertheless, the dose equivalent *H* per Gy delivered at the

This article has been accepted for publication in a future issue of this journal, but has not been fully edited. Content may change prior to final publication. Citation information: DOI 10.1109/TNS.2019.2943597, IEEE Transactions on Nuclear Science

BP in water increases with depth, because the absorbed dose is growing faster with depth compared to the decrease of $\bar{Q}$. Similarly, $\bar{Q}$ values behind the Al wall of 7.3 mm thickness (inside the spacecraft scenario) decrease faster at the BP position shifted at 57.3 mm depth in water. The change of H values with depth in astronauts, per Gy delivered at the BP in water, is presented in TABLE III. Values are higher at the same depth in astronauts in comparison to the dose equivalent outside of the spacecraft but this difference is not so compared to ^{16}O ions.

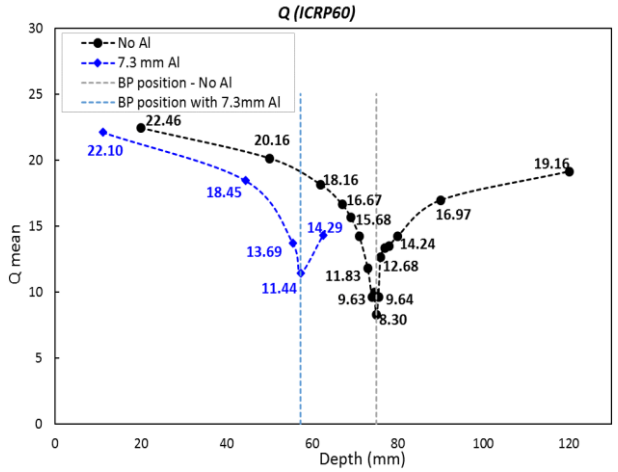

Figure 8. Quality factor Q at the same depths in water with and without 7.3mm Al wall, obtained with SOI microdosimeter in response to 500 MeV/u ^{56}Fe ions. Vertical dashed lines show the Brag Peak position at 57.3 mm depth in water and 75 mm depth in water, respectively with and without 7.3 mm Al wall.

IV. Conclusion

The response of an SOI "mushroom" microdosimeter developed by the CMRP was investigated with high-energy ions at HIMAC (Japan) typical for GCR. Two irradiations were carried out with 400 MeV/u ^{16}O ions and 500 MeV/u ^{56}Fe ions, in a free air geometry and in a water phantom with and without the presence of aluminum slabs representing the wall of a spacecraft. Two PMMA converters of 0.07 mm and 10 mm thick were put in front of the probe to mimic conditions for measurements of the dose equivalent Hp(0.07) and Hp(10). The aim was to study the hazard posed by heavy ions inside and outside a spacecraft to evaluate the effects of the wall's shielding material. Results including dose equivalent normalized to an absorbed dose in a BP and $\bar{Q}$ were obtained using the tissue-equivalent microdosimetric spectra obtained with mushroom microdosimeter. Oxygen ions became more harmful once they reached the inside of the spacecraft due to the high LET ions and secondaries produced while propagating through the Al and PMMA. On the contrary, iron ions are totally stopped by the 35.95 mm thick wall resulting in a lower $\bar{Q}$ and dose equivalent. If the wall thickness is reduced to 7.3 mm of Al, representing only the outer shell of the spacecraft and the "Internal Out-fitting" (devices made of aluminum inside the spacecraft) is not considered, iron ions propagate through the Al without being stopped or incurring significant fragmentation.

The $\bar{Q}$ values at different depths within the body of an astronaut were investigated with and without the presence of the aluminum wall, representing the two scenarios encountered in space, inside and outside the spacecraft. Due to the low *LET* of 19.38 keV/µm at the entrance depth of the water phantom, the $\bar{Q}$ value corresponding to oxygen ions is increasing with depth in a body according to Equation (2). Conversely, iron ions see a decrease of $\bar{Q}$ along depths of the human body because of the higher *LET* at the entrance depth of the water phantom (167.98 keV/µm), and its further increase after the BP. The presence of the shielding wall caused a shift of the Bragg Peak to more shallow depths in the water phantom, resulting in a more harmful exposure of superficial organs of the astronaut's body as in the case of oxygen and iron ions considered in this study (Table III). For two scenarios (inside and outside the spacecraft), the same organs of the astronaut body will have essentially different dose equivalent exposure that also depends on energy spectra and type of ions that is difficult to predict accurately and that emphasizes the importance of wearing personal microdosimeter during space mission.

To conclude, for wide energy ranges of GCR ions, the Al wall does not always reduce the radiation hazard inside the spacecraft. While stopping lower energy ions, the wall can attenuate the energy of primary ions and produce secondary particles. Particularly, the dose equivalent can increase at shallow depth but can be reduced (or increased further) deeper in the body of an astronaut.

This study confirms that the portable microdosimetric probe with SOI "mushroom" microdosimeter is suitable for quantifying the quality of the radiation field in space in terms of $\bar{Q}$, as well as evaluating the efficiency of shielding materials in terms of H. Results have been validated with Geant4 simulations, confirming the feasibility of using SOI microdosimeter for space application. While the dose to astronauts during deep space mission, like planned to Mars (about 360 days round trip), is expected to be 1÷3Gy [17-19], the radiation damage to silicon devices is not an issue especially for SOI devices [7], making the microdosimeter "mushroom" an attractive choice for personal dosimeters for astronauts.

V. Acknowledgment

We would like to thanks the Australian Research Council (ARC) for supporting this research with a Discovery Project Grant "Development of radiation detectors to better understand ion interactions" (DP 170102273), and European Space Agency (ESA) grant "Tissue-equivalent crew dosimeter based on novel 3D Si processing", (Contract No. 4000112670/14/NL/HK).

This work was also supported by computational resources provided by the Australian Government through the Raijin cluster under the National Computational Merit Allocation Scheme.

VI. References

[1] W. Suparta and S. K. Zulkeple, "Spatial Analysis of Galactic Cosmic Ray Particles in Low Earth Orbit/Near Equator Orbit Using SPENVIS," *Journal of Physics: Conference Series,* vol. 495, no. 1, pp. 1-6, 2014, Art. no. 012040.

[2] A. Wroe *et al.*, "Microdosimetry simulations of solar protons within a spacecraft," *IEEE Transactions on Nuclear Science,* vol. 52, no. 6, pp. 2591-2596, 2005.

[3] B. Gersey, S. Aghara, R. Wilkins, J. Wedeking, and R. C. Dwivedi, "Comparison of a Tissue Equivalent and a Silicon Equivalent Proportional Counter Microdosimeter to High-Energy Proton and Neutron Fields," *IEEE Transactions on Nuclear Science,* vol. 54, no. 6, pp. 2276-2281, 2007.

[4] L. Pinsky *et al.*, "Medipix in space on-board the ISS," *Journal of Radiation Research,* vol. 55, pp. 62-63, 2014.

[5] H. H. Rossi and M. Zaider, Springer, Ed. *Microdosimetry and Its Applications*. 1996.

[6] A. Rosenfeld, "Novel Detectors For Silicon Based Microdosimetry, Their Concepts And Applications," *Nuclear Instruments and Methods in Physics Research Section A: Accelerators, Spectrometers, Detectors and Associated Equipment,* vol. 809, pp. 156-170, 2016.

[7] B. James *et al.*, "SOI Thin Microdosimeter Detectors for Low Energy Ions and Radiation Damage Studies," *IEEE Transactions on Nuclear Science,* vol. 66, no. 1, pp. 320-326, 2018.

[8] L. T. Tran *et al.*, "Thin Silicon Microdosimeter Utilizing 3-D MEMS Fabrication Technology: Charge Collection Study and Its Application in Mixed Radiation Fields," *IEEE Transactions on Nuclear Science,* vol. 65, no. 1, pp. 467-472, 2018.

[9] L. T. Tran *et al.*, "3D Silicon Microdosimetry and RBE Study Using C-12 Ion of Different Energies," *IEEE Transactions on Nuclear Science,* vol. 62, no. 6, pp. 3027-3033, 2015.

[10] D. Bolst *et al.*, "RBE study using solid state microdosimetry in heavy ion therapy," *Radiation Measurements,* vol. 106, pp. 512-518, 2017.

[11] S. Guatelli *et al.*, "Tissue Equivalence Correction in Silicon Microdosimetry for Protons Characteristic of the LEO Space Environment," *IEEE Transactions on Nuclear Science,* vol. 55, no. 6, pp. 3407-3413, 2008.

[12] D. Bolst *et al.*, "Correction factors to convert microdosimetry measurements in silicon to tissue in (12)C ion therapy," *Phys Med Biol,* vol. 62, no. 6, pp. 2055-2069, Mar 21 2017.

[13] D. Bolst, L. T. Tran, S. Guatelli, N. Matsufuji, and A. B. Rosenfeld, "Modelling the Biological Beamline at HIMAC using Geant4," *Journal of Physics Conference Series,* vol. 1154, no. 1, pp. 1-6, 2019, Art. no. 012003.

[14] L. Chartier *et al.*, "New silicon microdosimetry probes for RBE and biological dose studies using stationary and movable targets in12C ion therapy," *Journal of Physics: Conference Series,* vol. 777, pp. 1-4, 2017, Art. no. 012019.

[15] R. Destefanis *et al.*, "Space environment characterisation of Kevlar®: good for bullets, debris and radiation too," *Universal Journal of Aeronautical & Aerospace Sciences,* vol. 2, pp. 80-113, 2014.

[16] M. Silvestri *et al.*, "Impact of Spacecraft-Shell Composition on 1 GeV/Nucleon 56Fe Ion-Fragmentation and Dose Reduction," *IEEE Transactions on Nuclear Science,* vol. 58, no. 6, pp. 3126-3133, 2011.

[17] L. Walsh *et al.*, "Research plans in Europe for radiation health hazard assessment in exploratory space missions," *Life Sci Space Res (Amst),* vol. 21, pp. 73-82, May 2019.

[18] C. Zeitlin *et al.*, "Measurements of energetic particle radiation in transit to Mars on the Mars science laboratory," *Science,* vol. 340, no. 80, pp. 1080-1084, 2013.

[19] J. C. Chancellor, G. B. I. Scott, and J. P. Sutton, "Space Radiation: The Number One Risk to Astronaut Health beyond Low Earth Orbit," *Life,* vol. 4, pp. 491-510, 2014.